



# White lead: A new naturally occurring 2D material

Pranay Ranjan<sup>1,2</sup>, Prashant Kumar<sup>2,3,a)</sup> 

<sup>1</sup>Department of Metallurgical and Materials Engineering, Indian Institute of Technology Jodhpur, Karwar, Rajasthan 342037, India

<sup>2</sup>Indian Institute of Technology Patna, Bihta Campus, Patna 801103, India

<sup>3</sup>Global Innovative Centre for Advanced Nanomaterials, School of Engineering, Faculty of Engineering and Built Environment, The University of Newcastle, Callaghan, NSW 2308, Australia

<sup>a)</sup>Address all correspondence to this author. e-mail: Prashant.Kumar@newcastle.edu.au; magmemory@gmail.com

Received: 3 June 2022; accepted: 6 July 2022; published online: 27 July 2022

**Atomic scale crystallographic structures of a quantum crystals depend on substrate, interfacial strain, defects, surface functionalities etc., which make it challenging to precisely control. To achieve high quality material, UHV conditions are prerequisite, which makes it costly. Naturally occurring 2D materials have tremendous significance in this regard. White lead, having weak interlayer coupling and easily found in natural ores have never been exfoliated. Keeping the novelty in mind, one needs to explore its physical as well as chemical behaviour and look out for appropriate applications. We for the first time, therefore, have sonochemically exfoliated white lead, and established its physical and chemical behaviour. We have also blended it with graphene oxide and explored its gas sensing applications and found the hybrid system to be very selective for NH<sub>3</sub> gas. White lead, a naturally occurring 2D material; has been exfoliated for the first time and its hybrid with graphene oxide has been explored for gas sensing.**

## Introduction

Atomically thin crystals, popularly known as two-dimensional (2D) materials exhibit quantum character. Graphene was the first explored 2D material and due to the least defect level and electron cloud over the crystal, electron transport is ballistic in graphene and therefore has been employed in ultrafast gas/light/strain sensors [1–3]. Apart from graphene, 2D materials consists of Xenes (phosphorene, borophene, 2D gold etc.), Transition metal oxides (TMOs), transition metal dichalcogenides (TMDCs), Transition metal carbides and nitrides (MXenes) and BN [4–15]. While various ways of synthesis of 2D materials have been explored, integration of 2D materials with other 3D/2D/1D/0D materials have been developed for enhanced device functionalities in recent years [16–25]. Scalability, reproducibility, economic cost of production and device integration issues are being worked out to excel in functionalities. Since fast and high response to stimuli, cyclability and lifetime of devices are dependent on electronic mobility, thermal conductivity, carrier concentration, structural stability etc., therefore intense research is ON to explore new 2D materials and novel functionalities and applications.

Naturally occurring 2D materials are of intense research interest as they are abundantly available in nature in highly crystalline form at economic price and therefore synthesis cost is curtailed. Among naturally occurring 2D materials, graphite, Franckeite [26], Hematene [27] and Ilmenene [28] have already been reported and they constitute new class of 2D materials (see Fig. 1). White lead, also known as Cerussite is one of the naturally occurring layered material [29, 30]. Due to its robustness against thermal as well as pressure conditions, white lead as a material has already been utilized in various applications including lubricants for gears in automobile and in aviation industries, as pigments in white paint and as insulating barriers in electronic industries [31, 32]. However, owing to high surface area and due to hydroxyl functionalities, it is also expected to be excellent for gas sensing applications. After a careful literature search, we arrived at a conclusion that white lead itself has never been exfoliated and its applications, especially in gas sensing applications has not yet been realized. In contrast, functionalized graphene sheet obtained from chemical processing of another naturally occurring 2D crystal (i.e., graphite); itself is a promising candidate for gas sensing applications [33–40]. However, at elevated thermal conditions its ionic character degrades

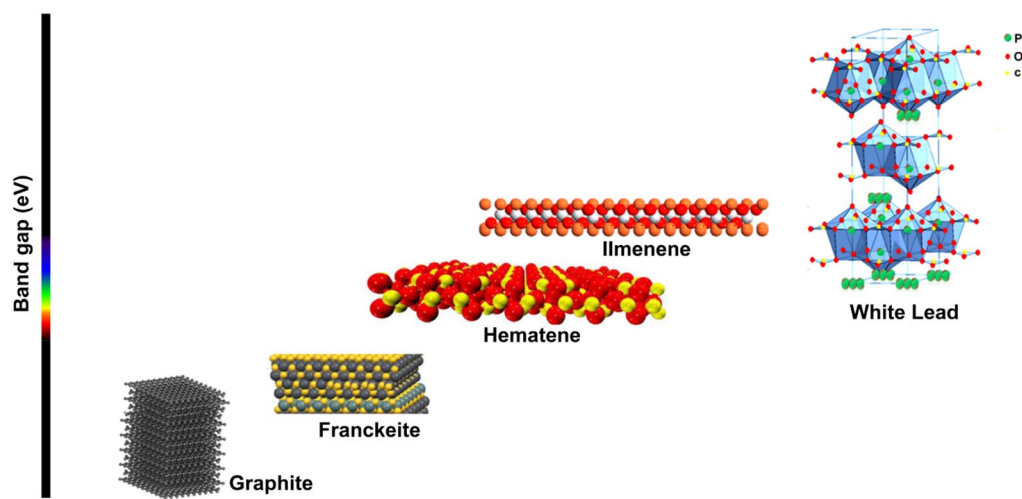


**Figure 1:** Glossary for family of naturally occurring 2D materials.

and its electronic character shines [41–47]. Thus, apart from establishing white lead as a new layered material with potential for sensing applications, there is an urgent need for the development of magic combinations (hybrids) of graphene oxide with thermally stable white lead, which can withstand extreme operating conditions and improved electronic behaviour of graphene oxide at elevated temperature (due to reduction) would help in giving sensing signal.

Assessing the urgent need to establish white lead as a new 2D material and to investigate its applications, we have investigated for the first time sonochemical exfoliation of white lead in deionised water solvent at room temperature. The as-synthesized material was characterized using a host of microscopic techniques such as optical microscopy, Atomic force microscopy (AFM) and transmission electron microscopy (TEM) as well as spectroscopic techniques such as Raman, X-ray photoelectron spectroscopy (XPS), Fourier transform infra-red (FTIR), UV–Visible and photoluminescence (PL) spectroscopy. To exploit attributes of graphene oxide (GO) and white lead (WL) together, we synthesized their hybrids by hybridizing chemically synthesized graphene oxide via adaptation of modified Hummer’s method with layered sheets of white lead synthesized via sonochemical exfoliation. Further, WL-GO hybrid has been explored for ammonia sensing.

White lead is a crystalline compound having layered structure [see Fig. 2(b)]. However, its molecular layers have never been exfoliated and therefore, behaviour of this material upon exfoliation is yet to be established. In order to exfoliate it, we employed sonochemical approach [see Fig. 2(a)]. After several hours (upto 30 h) of sonication, dispersion of white lead in deionised water solvent was centrifuged and supernatant was used for characterizations (microscopy as well as spectroscopy). Sheets attained have large distribution in thickness as seen in

atomic force microscopic image [Fig. 2(c)]. While the thinnest visible sheets were ~2 nm in vertical dimension and corresponding lateral dimension was ~100 nm, thicker sheets were ~4 nm in vertical dimension and ~130 nm lateral dimension (see line profiles at three locations in AFM image in Fig. 2(c) and Fig. S1, Fig. S2 in ESI). White lead, having carbonate and hydroxyl groups attached to lead, is expected to have local  $sp^3$  like behaviour and strain in the system due to which crumpling is expected and indeed we could visualize them in transmission electron microscopic image [see Fig. 2(d)]. Moreover, as compared to elemental 2D materials where there are no functionalities attached, this material is a compound sheet and hence will have its sheet relatively thicker. While Raman spectroscopy carried out on synthesized individual WL powder sample [optical image (inset in Fig. 2(e))] shows white colour coating on  $SiO_2/Si$  substrate) exhibits peaks at  $1050\text{ cm}^{-1}$  [see Fig. 2(e)] [48]. As can be established from XPS spectrum full scan survey [see Fig. 2(f)] and also in C1s [see Fig. 2(g)] and Pb  $4p_{3/2}$  [see Fig. 2(h)] peaks, synthesized sheets predominantly constitutes of lead carbonate (validation comes from XPS peak ~288.5 eV) along with signature of hydrocarbon [see Fig. 2(g), the O1s of the WL sheet is represented in Fig. S4 in ESI]. Photoresponse of WL thin films coated on ITO substrate has been obtained in presence of red laser and indeed it shows positive photoresponse, which might be due to hydroxyl removal owing to localized heating [see Fig. 2(i)]. This is being validated by power dependent enhancement in conductivity of the sample.

As both the component materials (GO as well as WL) are soluble in water due to available functionalities, to attain hybrids of WL with GO; therefore, supernatants of WL and GO in deionised water solvent were mixed together and sonicated for 30 min [see schematic in Fig. 3(a)]. Photograph of three bottles [see Fig. 3(b)], first one contains sonicated dispersion just

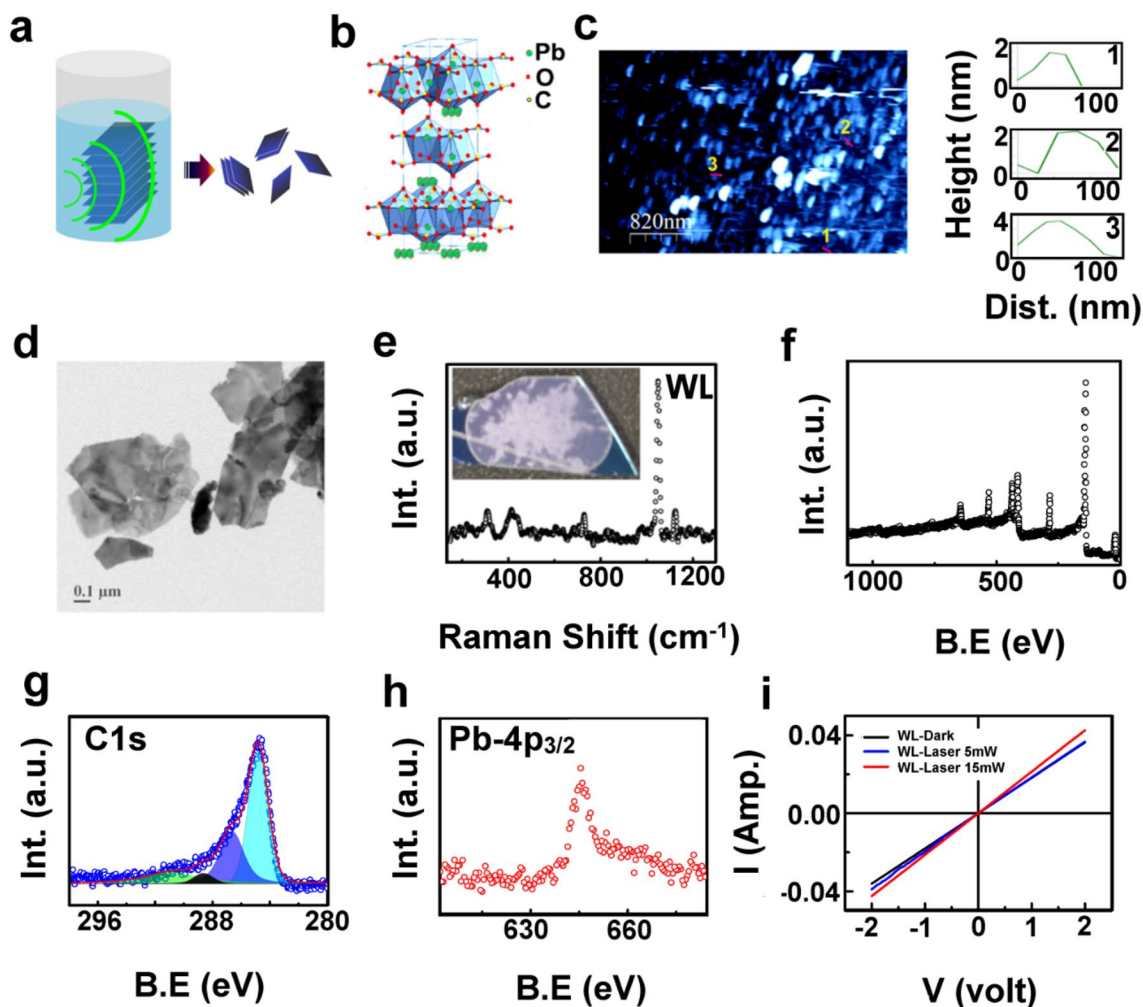


**Figure 2:** (a) Schematic diagram of sonochemical exfoliation of WL, (b) crystal structure, (c) AFM image, (d) TEM image, (e) Raman spectra (inset is photograph of WL coating on Si/SiO<sub>2</sub> substrate), (f) Full scan XPS spectra, (g) C1s XPS spectra, (h) PB-4p<sub>3/2</sub> spectra of WL atomic sheets and (i) I-V characteristic of WL sheets with different laser power (0, 5 and 15 mW).

before centrifugation, second one is the supernatant attained after the centrifugation and third one is WL-GO hybrid dispersed in deionised water. Once they are brought together in a sonicator, both WL and GO interact well with water and make homogeneous dispersion. TEM image of graphene oxide sheets attained by chemical route used for the purpose of hybridization is shown in Fig. 3(c) and exhibits folds and wrinkles which are characteristics of monolayers. Moreover, GO sheets are electron transparent as well. Selected area electron diffraction shows hexagonal pattern, diffused though which indicates defects in crystal structure of GO [see inset of Fig. 3(c)]. Raman spectrum of WL exhibits peak at 1050 cm<sup>-1</sup>, while GO exhibits Raman peak at 1344 cm<sup>-1</sup> (D band), 1595 cm<sup>-1</sup> (G band) and 2687 cm<sup>-1</sup> (2D band) [49–53]. WL/GO hybrid exhibits Raman peak at 1045 cm<sup>-1</sup>, 1337 cm<sup>-1</sup>, broad peak ~ 1570–1610 cm<sup>-1</sup>, and very broad 2D peak (2500–3000 cm<sup>-1</sup>) respectively [see Fig. 3(d)]. Raman peak shifts for G and 2D peaks (in WL-GO hybrid as

compared to GO) attests to the hybridization of orbitals. We have observed peak broadening for G-peak. Upon deconvolution, one can apparently observe G-peak splitting into three components. Original peak ~ 1595 cm<sup>-1</sup> of GO and softened peak ~ 1577 cm<sup>-1</sup> (which may arise due to hybridization with other materials [54] as well as one hardened peak ~ 1610 cm<sup>-1</sup> (which can be attributed to surface functionalities). Broad 2D peak arises due to residual strain in the systems due to hybridization and due to possible local out-of-plane features in such systems. To confirm this FTIR spectroscopy pin-pointedly was carried out. FTIR spectra of WL, GO and hybrid of WL/GO has been shown in Fig. 3(e). We observed shifts in FTIR peaks corresponding to –C–O– from 1000 to 1007 cm<sup>-1</sup>, –C=C– from 1620 to 1642 cm<sup>-1</sup> has been seen. However, peak corresponding to WL at 1363 cm<sup>-1</sup> has shifted to 1390 cm<sup>-1</sup> in hybrid material. FTIR peaks in WL-GO hybrid system are highly reduced as compared to that of GO, which confirms partial reduction

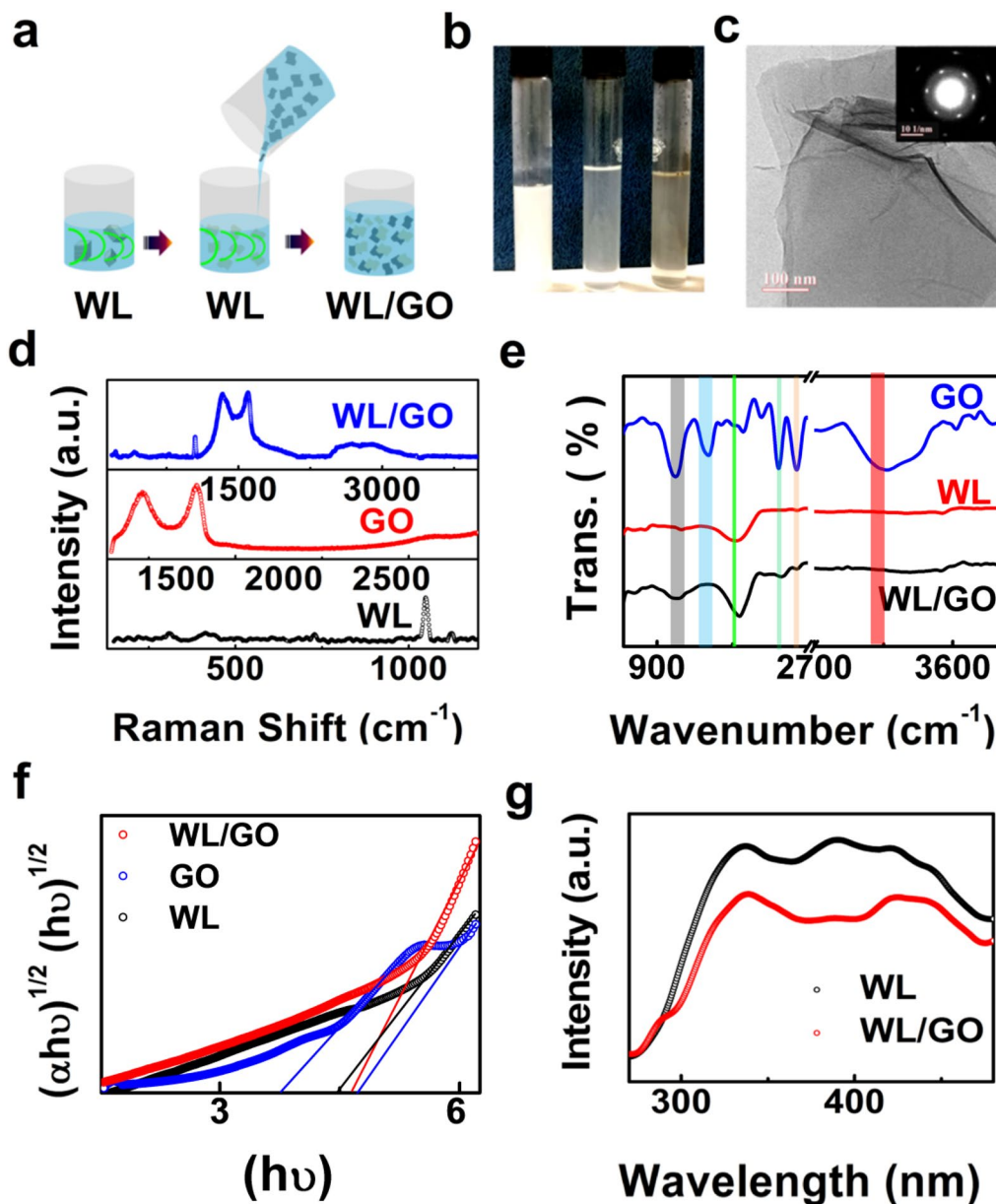


**Figure 3:** (a) Schematic diagram for synthesis of WL/GO hybrid, (b) Camera image of WL, GO and WL/GO hybrid sheets inside bottle after centrifugation, (c) TEM and SAED image of GO, (d) Raman, (e) FTIR and (f) UV-Vis spectra of WL, GO and WL/GO hybrid sheets and (g) PL spectra of WL and WL/GO hybrid.

of GO. Also, FTIR shifts also support Raman results as far as hybridization of orbitals is concerned. Hybridized orbitals of WL and GO are expected to result in physical and chemical behaviour of hybrid in between the individual component materials. GO exhibits UV-Vis absorption peak  $\sim 230$  nm ( $\pi-\pi^*$ ) and a shoulder  $\sim 265$  nm ( $n-\pi$ ) [55]. Upon excitation with 250 nm light, we could observe photoluminescence peaks for WL at  $\sim 335$  nm and  $\sim 370$  nm (in UV range) and at  $\sim 410$  nm and  $\sim 430$  nm (in visible range) [see Fig. 3(f)]. WL material being a high bandgap semiconductor (as evidenced by  $M\Omega$  resistance

in electrical measurements, discussed later), we expected PL peaks in UV range and indeed we attained PL peaks which correspond to  $\sim 4.7$  and  $\sim 3.7$  eV, respectively [see Fig. 3(g)].

Dissolved ammonia is routinely employed by farmers to improve nitrogen content of the soil which eventually would improve its fertility. However excessive usage can render the soil wasteland and endanger health (respiratory system disorder, irritation in eyes and even death) of the farmer. Therefore, safety standard level is 50 ppm of ammonia as per environmental safety standard [56]. However, detection of ammonia is



challenging in dissolved form. Lead having variable oxidation states namely +2 and +4, it would be worth watching how surface electrostatics in WL can be exploited for room temperature gas sensing, especially nitrous gases. White lead was therefore investigated for sensing of dissolved ammonia at room temperature. However, white lead itself did not respond to ammonia at room temperature which might be attributed to absence of sufficient electronegative surface-active sites needed for ammonia sensing. In contrast, GO contains many functional groups at its basal plane (surface active sites). Therefore, we employed hybrid of WL and GO for the purpose. To understand how the hybrid behaves as far as its sensitivity is concerned, we have compared its performance with that of GO layer itself. Figure 4 (a) and (c) represents the schematic diagram of GO and WL/GO hybrid molecular sheets as ammonia sensor. Figure 4 (b) shows the change in resistance ( $21\text{ M}\Omega$  to  $4\text{ M}\Omega$ ) of the GO film inside the chamber, when ammonia of different concentration (ranging from 26.4 ppm to 105.8 ppm) was exposed to it. At each step, recovery of the molecular sheet from ammonia was achieved by degassing it (employing vacuum pump) instead of heating. This helps in retaining all functional groups attached to GO which otherwise would be removed upon heating. The sensitivity of GO film has been calculated using  $R_{\text{NH}_3}-R_0/R_0$ ,

where  $R_{\text{NH}_3}$  and  $R_0$  are the resistances of the film after and before it was exposed to ammonia respectively. The response time of GO film at 26.4 ppm was found to be 7 s and recovery time of 146 s. While at 52.8 ppm, 79.4 ppm and 105.8 ppm the response times is 190 s, 438 s, 383 s respectively and their recovery times are 32 s, 109 s and 337 s, respectively [see Fig. 4(b)].

In contrast to GO film, GO-WL hybrid performs far better (in terms of response and recovery time) [see Fig. 4(b)]. A change in resistance of  $21\text{ M}\Omega$  to  $0.16\text{ M}\Omega$  has been recorded for GO-WL hybrid film at 26.4 ppm of ammonia, while its response and recovery time was found to be 7 s and 23 s, respectively. As GO contains various oxygen functional group and therefore is hydrophilic in nature, it is highly sensitive to slightest presence of moisture in atmosphere. Water molecule upon chemisorption, would split into  $\text{H}^+$  and  $\text{OH}^-$ .  $\text{H}^+$  would attach with oxygen functionality which will reduce the sheet resistance. GO in general behaves like an insulator, however when hybridized with WL (as evidenced by G- peak shift in Raman spectroscopy), GO will turn semiconducting which will enhance electronic character and hence efficient and prompt response to the analyte. While some of the remnant functional groups attached to GO will interact and hybridize with WL functionalities, others will disappear in the process, rendering GO more electronically

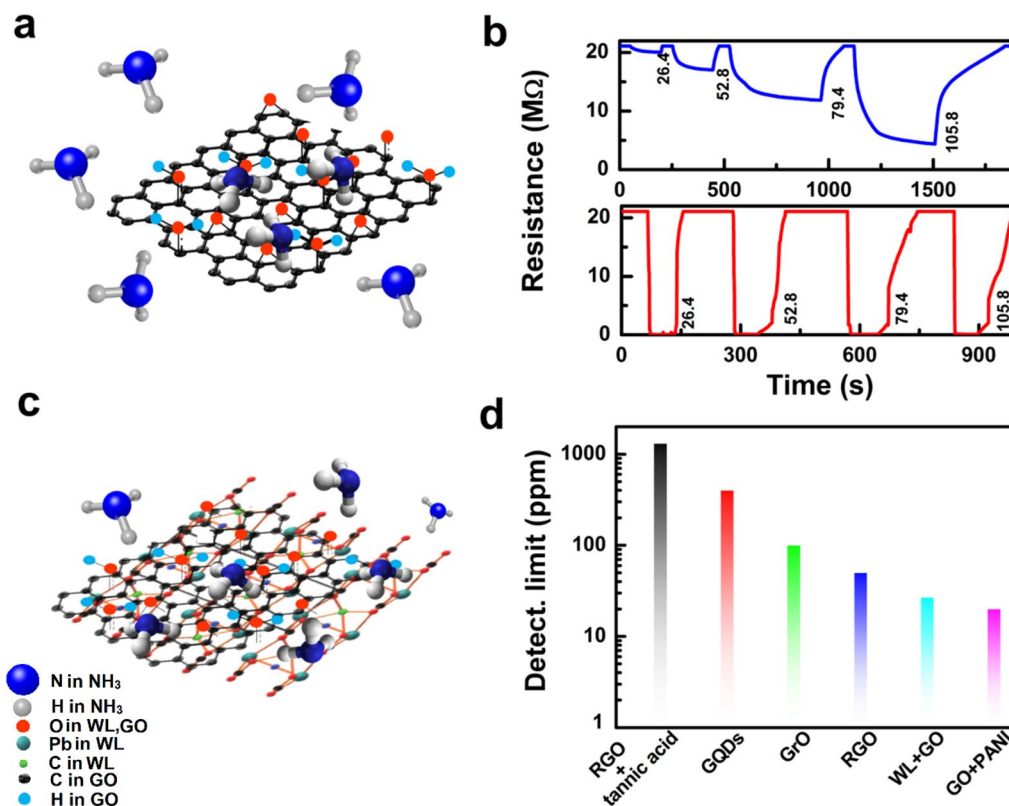


**Figure 4:** Schematic diagram demonstrating interactions of ammonia molecules with (a) GO and (c) WL/GO, (b) response of GO and WL/GO in presence of ammonia at different PPM levels (blue graph) and repeatability upto 5 cycles (red graph) and (d) comparison of sensitivity of gas sensing for WL/GO hybrid system in comparison to the existing 2D materials in literature.

conducting which helps charge collection faster. Mean the while; presence of WL makes the hybrid thermally robust as well. Carbonate group present in hybrid renders the surface electrophilic and ammonia is rich in electron. That is why, while GO film is sensitive to almost all volatile organic compounds (VOCs) (e.g. hydrogen peroxide, acetone, ethanol, iso-propyl alcohol) and in contrast to it, WL-GO hybrid is selective only to ammonia. Comparisons for ammonia detection limit achieved for WL-GO hybrid nanosystems as observed in the present research vis-à-vis those of nanomaterials (already reported earlier) are presented in Fig. 4(d) [57–61]. Even though GO along with polymers exhibit high detection limit, however those combinations are not thermally stable. In this aspect therefore, WL-GO hybrid emerges as robust magic material combination which has shown tremendous promise for gas detection, especially for nitrous gases.

As has earlier been evidenced by Raman as well as FTIR peak shifts, it has been established that WL hybridizes with GO. Essentially, WL and GO atomic sheets come close to each other due to van-der Waal interactions and as a result, their  $p_z$  orbitals overlap with each other. Such orbital overlap can even pull the atoms out-of-plane or out-of-plane bonding can occur as well. However, such vertical binding will be localized though. As soon as ammonia molecule lands on the GO surface (invited by oxygen functionalities), electronic exchanges occur at the surface, and it moves from one plane (GO) to other plane (WL) via cross-linkages established by orbital hybridization. Such prompt electrostatic charge draining gives prompt electronic signal giving rise to enhanced sensitivity [see Fig. 5(a)]. Fast removal of electrostatic surface charges leads to thinning of space charge layer at the surface. The band diagram corresponding to interaction of the surface with ammonium hydroxide before and after (in ambient conditions) are shown in Fig. 5(b). The reason of poor sensitivity of GO vis-à-vis WL/GO hybrid can also be

traced to compromised permeability of water in WL/GO hybrid as compared to that for GO layers [see the details in schematic diagram in Fig. 6(b) and 6(d)]. In order to validate it, we carried out contact angle measurement and we observed that while GO is hydrophilic in nature, WL in contrast is hydrophobic [see Fig. 6(a) and (c)]. In case of GO, as water molecules would impinge at the interface, it would rather weaken the inter-layer interactions and thereby increase the inter-layer distance; leading to poor sensitivity as compared to WL/GO hybrid. A comparison of WL/GO sheets with other oxidizing and reducing gases has been represented in Fig. S3 in ESI.

In conclusion, white lead, one of the naturally occurring 2D material has been exfoliated for the first time by sonochemical approach and its potential for gas sensing application has been explored. Monolayers as well as molecular sheets consisting of few monolayers of WL having lateral dimensions in 50 nm to 1.5  $\mu\text{m}$  range have been evidenced to form. While Raman and XPS spectroscopy attested to chemical phase purity, UV-Vis and PL spectroscopy hints at WL having bandgap of  $\sim 4.7$  eV. In order to explore gas sensing applications, especially for nitrous gases (e.g. ammonia); WL has been blended with graphene oxide. FTIR spectroscopy carried out on the hybrid material hints at eventual reduction of GO, which has been boon in disguise as it has helped in enhancing measurement sensitivity. Interestingly, hybridization of orbitals of WL and GO (as has been evidenced in Raman and FTIR spectroscopy) makes the hybrid nanosystems a unique platform. WL-GO hybrid possesses the following attributes: (a) presence of the channels for electrostatic charge draining, (b) thermal robustness in comparison to GO, (c) hydrophobic nature of WL in contrast to hydrophilic behaviour of GO. We observed that GO alone is not selective and suffers from several limitations, blending it with WL makes it uniquely suited for ammonia sensing with selectivity and enhanced sensitivity.

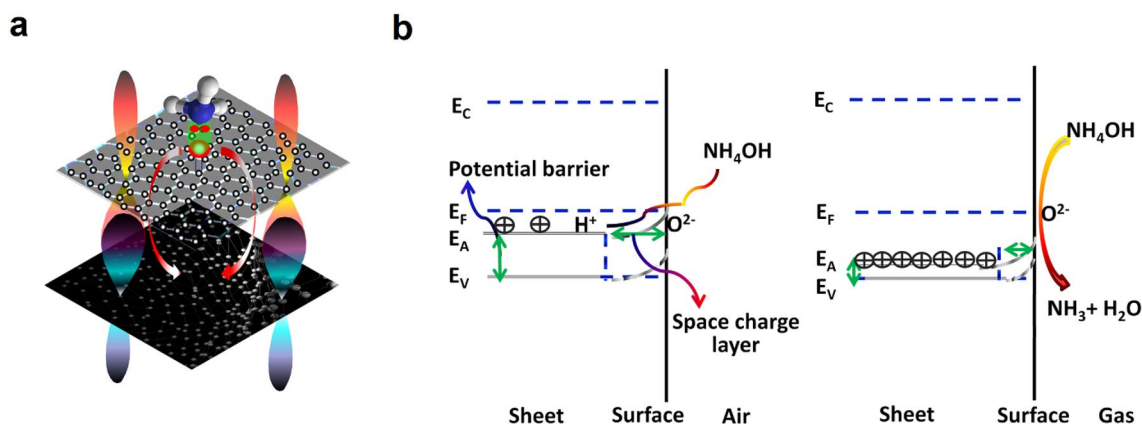


**Figure 5:** (a) Illustration of orbital overlapping/hybridization in GO and WL heterolayer, with ammonia molecule anchored on GO surface, (b) Band diagram of WL/GO on interaction with liquid ammonia.

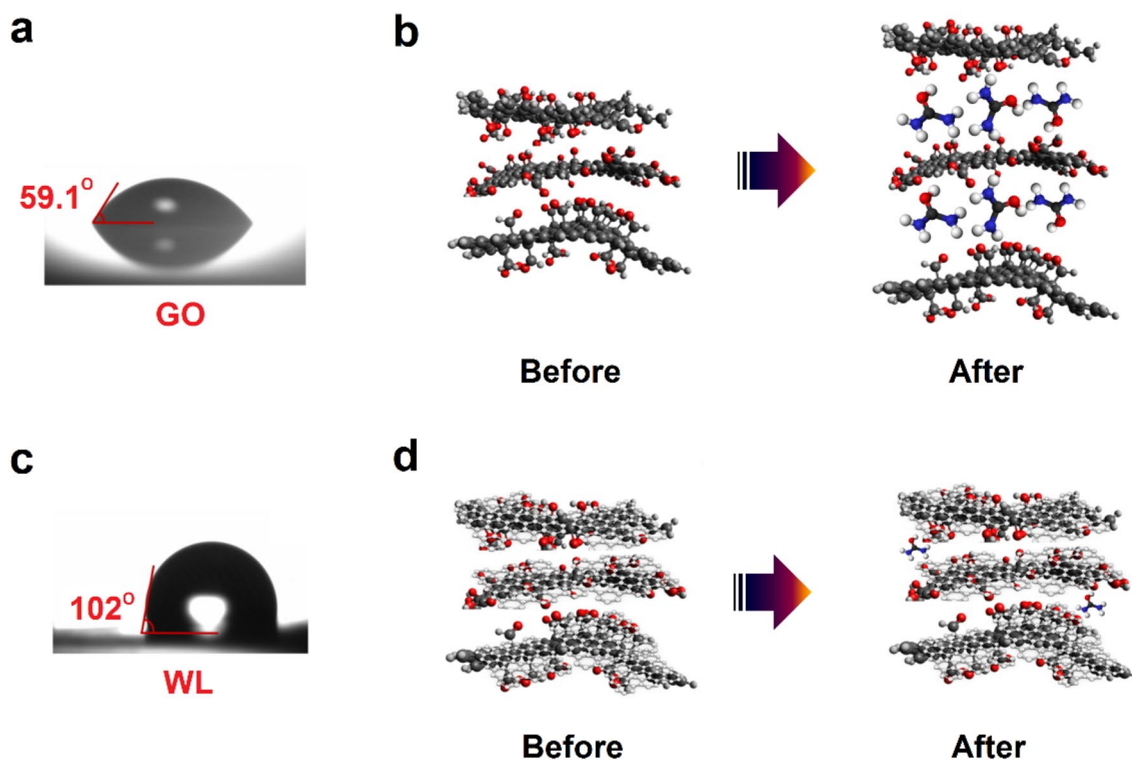


**Figure 6:** Sessile drop and confined contact angle measurement of (a) GO and (c) white lead drop casted on a sodium silicate substrate, schematic (3D view) depicting interlayer distance of (b) GO and (d) WL/GO before and after liquid ammonia (ammonium hydroxide) intercalation.

## Methods

### Chemicals

All the chemicals were purchased and used as received without any filtration or treatment from Sigma Aldrich and Alfa Aesar. Graphite was purchased from Alfa Aesar (purity-99.5%), Potassium permanganate ( $\text{KMnO}_4$ ) was purchased from Sigma Aldrich (purity-99%), Sulphuric acid ( $\text{H}_2\text{SO}_4$ ), Orthophosphoric acid ( $\text{H}_3\text{PO}_4$ ), hydrochloric acid (HCl) were purchased from Sigma Aldrich (purity-98%) and Hydrogen Peroxide ( $\text{H}_2\text{O}_2$ ) was purchased from Central Drug House Pvt. Ltd. (CDH, purity-30%). Distilled water was purchased from Merck (emplura, SI6SF66810).

### Synthesis of white lead

Cerussite obtained as a natural mineral (combination of lead hydroxide and lead carbonate) was sonicated for prolonged duration (upto 36 h) in deionised water (DI). The resultant dispersion was centrifuged at high speed (~5000 rpm) to remove heavy chunks and impurities. Upon centrifugation, supernatant was then sonicated and then centrifuged at 8000 rpm and the resulting supernatant was further

characterized. Supernatant was then vacuum dried to attain sheets of the layered white lead material.

### Synthesis of graphene oxide

Graphene oxide used for making 2D hybrid material has been synthesized using adapted improved Hummer's method. We have taken graphite (C) and potassium permanganate ( $\text{KMnO}_4$ ) in a ratio of 1:6 and prepared a fine mixture of it in a mortar and pestle and cooled below room temperature. Another solution of acids, containing sulphuric acid and hydrogen peroxide in a ratio of 9:1 was prepared and cooled at 5 °C. The admixture solution of acids and powder mixture of graphite and the  $\text{KMnO}_4$  powder was mixed and heated at elevated temperature followed by stirring. Finally, ice (400 gm) made up of deionized water (D.I) water was added to the solution and hydrogen peroxide was added. The solution was washed with water, ethanol and hydrochloric acid and then degassed for 8 h.

### Synthesis of white lead/graphene oxide hybrid

White Lead (WL) and graphene oxide (GO) was synthesized through sonochemical synthesis and chemical exfoliation

using an adaption over improved Hummer's method respectively. 200 mg of cerussite was dispersed in a bottle containing 100 ml solution DI water. The bottles were kept in ultrasonic bath and allowed to ultrasonicate for upto 36 h. After sonication the resulting fluids were centrifuged at 6000 rpm for 5 min and the supernatant were mixed with GO in a ratio 1:0.2 (wt%) and sonicated for 30 min and then characterized by transmission electron microscopy. It was observed that the supernatant contains less than 5 layers in each case.

## Characterization

**Optical Microscopy and Spectroscopy:** Bright and Transmission electron microscopy (TEM) from JEOL (JEM 2100) was used to obtain TEM, HRTEM and SAED of white lead and graphene oxide samples. Atomic force microscopy (AFM) (Agilent Model No.5500) was used in non-contact mode to estimate thickness of the synthesized sheets of white lead transferred on Si/SiO<sub>2</sub> substrate. X-ray Photoelectron spectroscopy (XPS) from ESCA + Omicron Nano Technology GmbH was employed in ultra high vacuum (UHV) conditions to characterize white lead sheets. Raman spectroscopy of white lead, graphene oxide and their hybrids sheets attained in aqueous solvent (DI Water) were carried out in the wave number range of 130–3500 cm<sup>-1</sup> in the back scattering geometry using confocal Micro-Raman Spectrometer (Seki Technotron Corporation, Japan) with 633 nm Helium neon LASER as excitation source by STR Raman Spectrograph. A 100X microscope from Olympus was used to focus the LASER beam and collect the light. The optical imaging of white lead sheets were done on an Olympus microscope integrated to confocal Micro-Raman Spectrometer. Functional groups attached to white lead, graphene oxide and their hybrids sheets were characterized in Fourier transform infrared spectroscopy (Shimadzu IrAfinity-1). The bandgap of white lead, graphene oxide and their hybrids sheets and their hybrids were calculated using UV-VIS spectroscopy (Perkin Elmer Lambda-35).

## Gas sensing

Free standing white lead sheets, graphene oxide sheets and their hybrids were dispersed in DI water and spin coated at 800 rpm on the sodium silicate substrate. The contacts on the films were made using silver wire and silver paint. The substrate (sodium silicate) used was cleaned by piranha cleaning before film deposition by spin coater followed by washing through DI water, ethanol, and acetone. The deposited films were kept under a sealed desiccator and were degassed at 10<sup>-3</sup> torr using rotary pump. Gas sensing measurements were performed on a laboratory customized chamber that has electrical feed through connections for electrical measurements

inside vacuum chamber. All the electrical measurement was done inside the vacuum chamber. Kiethley 2420 source meter instrument installed in Solar cell tester PET Cell Tester Model CT50AAA was used to measure change in resistance at room temperature (30 °C). Liquid ammonia (conc. 30%) analyte was inserted inside the desiccators using calibrated syringe through rubber cork. The concentration of analyte was converted into PPM using equation

$$C = \frac{22.4\rho TV_s}{273MT}$$

where C is defined as the concentration of gaseous ammonia (parts per million, ppm), T is the testing temperature or operating temperature (K), ρ is the density of liquid ammonia (g mL<sup>-1</sup>), V<sub>s</sub> is the volume of ammonia (μL), M is the molecular weight of ammonia (g mol<sup>-1</sup>) and v is the volume of the chamber (L). Change in current of the film was observed while different analyte concentration ranging from 26.8 ppm to 105.8 ppm was inserted and degassed. The response of the film was calculated using equation

$$\text{Response} = \frac{\Delta I}{I} = \frac{I_{\text{ammonia}} - I_0}{I_0}$$

where I<sub>0</sub> and I<sub>ammonia</sub> are the initial and final current value of the film on exposure to liquid ammonia.

## Acknowledgments

We acknowledge Department of Science and Technology, Govt. of India for Research grant under Ramanujan Fellowship (Sanction No. SB/S2/RJN-205/2014). We also acknowledge Indian Institute of Technology Patna for providing research facilities and Indian Institute of Technology Jodhpur for the seed grant.

## Author contributions

PK conceived the idea. PR carried out synthesis of white lead and its hybrids and gas sensing. PK and PR wrote the paper. PK oversaw the project.

## Funding

Open Access funding enabled and organized by CAUL and its Member Institutions. Funding was provided by Mission on Nano Science and Technology (SB/S2/RJN-205/2014).

## Data availability

Data are available on request from corresponding author.



## Declarations

**Conflict of interest** We declare no conflict of interests.

## Supplementary Information

The online version contains supplementary material available at <https://doi.org/10.1557/s43578-022-00655-6>.

## Open Access

This article is licensed under a Creative Commons Attribution 4.0 International License, which permits use, sharing, adaptation, distribution and reproduction in any medium or format, as long as you give appropriate credit to the original author(s) and the source, provide a link to the Creative Commons licence, and indicate if changes were made. The images or other third party material in this article are included in the article's Creative Commons licence, unless indicated otherwise in a credit line to the material. If material is not included in the article's Creative Commons licence and your intended use is not permitted by statutory regulation or exceeds the permitted use, you will need to obtain permission directly from the copyright holder. To view a copy of this licence, visit <http://creativecommons.org/licenses/by/4.0/>.

## References

1. F. Schedin, A.K. Geim, S.V. Morozov, E.W. Hill, P. Blake, M.I. Katsnelson, K.S. Novoselov, *Nat. Mater.* **6**, 652–655 (2007)
2. K.S. Novoselov, A.K. Geim, S.V. Morozov, D. Jiang, Y. Zhang, S.V. Dubonos, I.V. Grigorieva, A.A. Firsov, *Science* **306**, 666–669 (2004)
3. S. Pisana, M. Lazzeri, C. Casiraghi, K.S. Novoselov, A.K. Geim, A.C. Ferrari, F. Mauri, *Nat. Mater.* **6**, 198–201 (2007)
4. L. Li, J. Kim, C. Jin et al., *Nature Nanotech* **12**, 21–25 (2017)
5. A.J. Mannix, X.-F. Zhou, B. Kiraly, J.D. Wood, D. Alducin, B.D. Myers, X. Liu, B.I. Fisher, U. Santiago, J.R. Guest, M.J. Yacaman, A. Ponce, A.R. Oganov, M.C. Hersam, N.P. Guisinger, *Science* **350**, 1513 (2015)
6. P. Ranjan, T.K. Sahu, R. Bhushan, S.S.R.K.C. Yamijala, D.J. Late, P. Kumar, A. Vinu, *Adv. Mater.* **31**, 1900353 (2019)
7. P. Ranjan, J.M. Lee, P. Kumar, A. Vinu, *Adv. Mater.* **32**, 2000531 (2020)
8. S. Chahal, M. Motlag, S.S.R.K.C. Yamijala, D. J. Late, E.H.S. Sadki, G. J. Cheng, P. Kumar, *Adv Mater* **33**, 2102039 (2021).
9. P. Kumar, J. Liu, P. Ranjan, Y. Hu, S.S.R.K.C. Yamijala, S.K. Pati, J. Irudayaraj, G.J. Cheng, *Small* **14**, 1703346 (2018)
10. D. Lin, P. Kumar, S. Jin, S. Liu, Q. Nian, G.J. Cheng, *Appl. Surf. Sci.* **351**, 148–154 (2015)
11. S. Chahal, S.M. Kauzlarich, P. Kumar, *ACS Mater. Lett.* **3**, 631–640 (2021)
12. M. Amani et al., *Science* **350**, 1065 (2015)
13. A. Vahidmohammadi et al., *Science* **372**, eabf1581 (2021).
14. S.M. Kim et al., *Nat. Commun.* **6**, 8662 (2015)
15. S. Chahal, A. Bandyopadhyay, S.P. Dash, P. Kumar, *J. Phys. Chem. Lett.* (2022). <https://doi.org/10.1021/acs.jpclett.2c01540>
16. P. Kumar, S.S.R.K.C. Yamijala, S.K. Pati, *J. Phys. Chem. C* **120**, 16985–16993 (2016)
17. P. Kumar, A. Dey, J. Roques, L. Assaud, S. Franger, P. Parida, V. Biju, *ACS Mater. Lett.* **4**, 263–270 (2022)
18. S.R. Das et al., *ACS Nano* **9**, 11121–11133 (2015)
19. Y. Hu et al., *Nanoscale* **7**, 19885–19893 (2015)
20. J. Liu et al., *J. Phys. Chem. C* **119**, 6331–6336 (2015)
21. J. Liu et al., *Adv. Opt. Mater.* **9**, 2001830 (2021)
22. A. Qurashi et al., *J. Mater. Chem. C* **3**, 11959–11964 (2015)
23. K. Vishwakarma et al., *Phys. Chem. Chem. Phys.* **24**, 12816 (2022)
24. Y. Hu et al., *Adv. Opt. Mater.* **4**, 1811–1823 (2016)
25. P. Kumar et al., *Nano Lett.* **19**, 283–291 (2018)
26. A.J.M. Mendoza, E. Giovanelli, W.S. Paz, M.A. Nin, J.O. Island, C. Evangeli, L. Aballe, M. Foerster, H.S.J.V. Zant, G.R. Bollinger, N. Agrai, J.J. Palacios, E.M. Perez, A.C. Gomez, *Nat. Commun.* **8**, 14409 (2017)
27. A.P. Balan, S. Radhakrishnan, C.F. Woellner, S.K. Sinha, L. Deng, C.D.L. Reyes, B.M. Rao, M. Paulose, R. Neupane, A. Apte, V. Kochat, R. Vajtai, A.R. Harutyunyan, C.W. Chu, G. Costin, D.S. Galvao, A.A. Martí, P.A.V. Aken, O.K. Varghese, C.S. Tiwary, A.M.M.R. Iyer, P.M. Ajayan, *Nat. Nanotechnol.* **13**, 602–609 (2018)
28. A.P. Balan, S. Radhakrishnan, R. Kumar, R. Neupane, S.K. Sinha, L. Deng, C.A. Reyes, A. Apte, B.M. Rao, M. Paulose, R. Vajtai, C.W. Chu, G. Costin, A.A. Martí, O.K. Varghese, A.K. Singh, C.S. Tiwary, M.R. Anantharaman, P.M. Ajayan, *Chem. Mater.* **30**, 5923–5931 (2018)
29. S.V. Krivovichev, P.C. Burns, *Mineral. Mag.* **64**, 1077–1087 (2000)
30. V. Gonzalez, D. Gourier, T. Calligaro, K. Toussaint, G. Wallez, M. Menu, *Anal. Chem.* **89**, 2909–2918 (2017)
31. M. Montgomery, A. Mathee, *Environ. Res.* **98**, 279–283 (2005)
32. A.W. Anderson, *Anaconda Ind. Eng. Chem.* **26**, 1047–1049 (1948)
33. E. Gouda, I. Faquhi, S. Kariri, M. Qohal, Y. Kariri, *Int. J. Mater. Sci. Appl.* **4**, 8–11 (2015)
34. P. Ranjan, P. Tiwary, A.K. Chakraborty, R. Mahapatra, A.D. Thakur, *J. Mater. Sci.* **29**, 15946–15956 (2018)
35. S. Prezioso, F. Perrozzi, L. Giancaterini, C. Cantalini, E. Treossi, V. Palermo, M. Nardone, S. Santucci, L. Ottaviano, *J. Phys. Chem. C* **117**, 10683–10690 (2013)
36. S. Borini, R. White, D. Wei, M. Astley, S. Haque, E. Spigone, N. Harris, J. Kivioja, T. Ryhanen **7**, 11166–11173 (2013)
37. T.H. Han, Y.K. Huang, A.T.L. Tan, V.P. Dravid, J. Huang, *J. Am. Chem. Soc.* **133**, 15264–15267 (2011)

38. J.D. Fowler, M.J. Allen, V.C. Tung, Y. Yang, R.B. Kaner, B. H. Weiller **3**, 301–306 (2009)
39. H. Bai, K. Sheng, P. Zhang, C. Li, G. Shi, J. Mater. Chem. **21**, 18653–18658 (2011)
40. Y.H. Yang, L. Bolling, M.A. Priolo, J.C. Grunlan, Adv. Mater. **25**, 503–508 (2013)
41. P. Ranjan, S. Agrawal, A. Sinha, T.R. Rao, J. Balakrishnan, A.D. Thakur, Sci. Rep. **8**, 12007 (2018)
42. M. Lundie, Z. Sljivancanin, S. Tomic, J. Mater. Chem. C **3**, 7632 (2015)
43. C.G. Navarro, R.T. Weitz, A.M. Bittner, M. Scolari, A. Mews, M. Burghard, K. Kern, Nano Lett. **7**, 11 (2007)
44. M. Lundie, S. Tomic, Z. Sljivancanin, Phys. Scr. **162**, 014019 (2014)
45. S. Pei, H.M. Cheng, Carbon **50**, 3210–3238 (2012)
46. A. Bagri, C. Mattevi, M. Acik, Y.J. Chabal, M. Chhowalla, V.B. Shenoy, Nat. Chem. **2**, 581–587 (2010)
47. H. Wang, J.T. Robinson, X. Li, H. Dai, J. Am. Chem. Soc. **131**, 9910–9911 (2009)
48. L. Burgio, R.J.H. Clark, S. Firth, Analyst **126**, 222–227 (2001)
49. A. Kaniyoor, S. Ramaprabhu, AIP Adv. **2**, 032183 (2012)
50. J.B. Wu, M.L. Lin, X. Cong, H.N. Liu, P.H. Tan, Chem. Soc. Rev. **47**, 1822 (2018)
51. K.N. Kudin, B. Ozbas, H.C. Schniepp, R.K. Prud'homme, I.A. Aksay, R. Car, Nano Lett. **8**, 36–41 (2008)
52. D.L. Diaz, M.L. Holgado, J.L.G. Fierro, M.M. Velázquez, J. Phys. Chem. C **121**, 20489–20497 (2017)
53. J.S. Mehta, A.C. Faucett, A. Sharma, J.M. Mativetsky, J. Phys. Chem. C **121**, 16584–16591 (2017)
54. P. Ranjan, Tulika, R. Laha, J. Balakrishnan, J. Raman Spectrosc. **48**, 586–591 (2017).
55. J. Zhang, H. Yang, G. Shen, P. Cheng, J. Zhang, S. Guo, Chem. Commun. **46**, 1112–1114 (2010)
56. G. Eranna, CRC Press, Taylor and Francis Group, 2012, 13, 978-1-4398-6341-1.
57. Y. Wang, L. Zhang, N. Hu, Y. Wang, Y. Zhang, Z. Zhou, Y. Liu, S. Shen, C. Peng, Nanoscale Res. Lett. **9**, 251 (2014)
58. Z. Ye, Y. Chen, B. Liu, Y. Su, Z. Chen, H. Tai, Y. Jiang, ECS J. Solid State Sci. Technol. **7**, Q3148–Q3152 (2018)
59. S. Yoo, X. Li, Y. Wu, W. Liu, X. Wang, W. Yi, J. Nanomater. **2014**, 497384
60. A.G. Bannov, J. Prášek, O. Jašek, L. Zajíčková, Sensors **17**, 320 (2017)
61. W. Chen, F.L.P.C. Ooi, Y. Ye, T.W. Kim, T. Guo, Sens. Actuators B **222**, 763–768 (2016)